Oxygen-deficiency-activated charge ordering in $La_{2/3}Sr_{1/3}MnO_{3-\delta}$ thin films

J. Li[a] and C. K. Ong
Department of Physics, National University of Singapore, Singapore 119260

J.-M. Liu
Department of Physics, National University of Singapore, Singapore 119260 and Laboratory of Solid State Microstructures, Nanjing University, 210093, People's Republic of China

Q. Huang and S. J. Wang
Department of Physics, National University of Singapore, Singapore 119260

(Received 30 August 1999; accepted for publication 23 December 1999)

The oxygen-deficiency-activated charge ordering (CO) transition has been observed in C-oriented $La_{2/3}Sr_{1/3}MnO_{3-\delta}$ thin films prepared by pulsed laser deposition on $LaAlO_3$ substrates. A rapid growth of the sample resistivity at temperatures below T_C is observed, while significant thermal hysteresis and electrical field induced transition from the insulator CO state to metallic-like state are recorded. Such a CO state can also be partially melted under a magnetic field of 0.4 T, resulting in enhanced magnetoresistance at low temperatures. Magnetic properties of the films can be well understood as the coexistence of the ferromagnetic state and the CO state. The CO state in oxygen deficient thin films is explained in terms of the Mn–O octahedral distortion or the narrowness of the conduction bandwidth of the e_g carriers. © *2000 American Institute of Physics.* [S0003-6951(00)04008-0]

Recently, charge/orbital ordering (CO) state is found prevalent in doped perovskite manganite systems such as $Pr_{1-x}Ca_xMno_3$, $Nd_{1-x}Sr_xMnO_3$, and $Sm_{1-x}Sr_xMnO_3$, especially when the hole concentration takes the commensurate values, e.g., $x=1/3$, 1/2, or 2/3.[1–3] Upon the CO phase transition, the resistivity may have a jump up to several orders of magnitude, and simultaneously the so-called double exchange (DE) ferromagnetic-metallic state transforms into an antiferromagnetic state. It is shown that the CO represents a charge localization state, in which Mn^{3+} and Mn^{4+} species align alternatively into a real spatial lamellar structure along *c* axis of the orthorhombic lattice, and the collinear homovalent Mn spins couple to each other antiferromagnetically.

Several parameters are known to influence the CO sequence significantly, among which the most crucial one is the one-electron bandwidth *W*. The reduction in *W* favors the CO state, while destabilising the ferromagnetic state.[2] The magnitude of *W* decreases with increasing Mn–O octahedral distortion (or decreasing tolerant parameter *f*). In short, the bandwidth is narrowed with expansion of the Mn–O bond length and bending of the Mn–O–Mn bond. It is therefore quite understandable that the CO transition was observed in several experiments where either the average ionic radius of A site ($\langle \gamma_A \rangle$) was reduced or an external pressure was applied.[2,5]

Serious lattice distortion in oxygen deficient manganite thin films is generally observed. The oxygen deficiency may also lead to the distortion of the Mn–O octahedral thus decrease *W*, quite similar to the effect of decreased $\langle \gamma_A \rangle$. As the result of reduced *W* as well as reduced carrier density, the sample resistivity increases and the Curie temperature T_C at which DE occurs shifts to lower temperatures, as previously reported.[6–10] Therefore, it is possible to activate the CO state by controlled oxygen deficiency, although such a phenomenon has never been reported up to date. In this letter, we report our preliminary confirmation of this argument in well prepared but oxygen deficient $La_{2/3}Sr_{1/3}MnO_3$ thin films. We chose this system because the oxygen stoichiometric sample ($\langle \gamma_A \rangle \approx 1.24$ Å and $f \approx 0.975$) posses a large *W* value (or weak lattice distortion).[4] It behaves like a ferromagnetic metal over a wide temperature range up to 360 K. Therefore, the CO phenomenon observed can be solely attributed to oxygen deficiency of the sample.

The epitaxial thin films were prepared on (001)-$LaAlO_3$ (ALO) substrates by pulsed laser deposition. The laser fluency was 2.0 J/cm^2 with a reprate of 3 Hz. The substrate temperature was 700 °C during deposition. Then, the film was kept *in situ* for 0.5 h before slowly cooled down. Various oxygen pressures (P_O) from 6.5×10^{-4} to 0.45 mbar were adopted during deposition and subsequent cooling procedure in order to control the oxygen deficiency, as well established previously.[10] An oxygen stoichiometric sample was obtained by postannealing the $P_O=0.45$ mbar film at 800 °C in 1 atm O_2 for 1.5 h. Thickness of all the thin films remains to be 100–200 nm, x-ray diffraction (XRD) investigation indicates that all the films are completely *c*-axis oriented.

We first present in Fig. 1 the zero-field resistivity (ρ_0) as a function of temperature (*T*) for samples deposited at different P_O. Inset is the ρ_0-*T* curve of our stoichiometric sample, which shows T_C at about 345 K, slightly lower than the bulk data (360 K) reported.[5] Pronounced effect of the oxygen deficiency on the electrical transport properties is demonstrated. Careful investigation shows that behavior of the samples deposited at 0.45, 0.15, and 6.5×10^{-4} mbar is concordant with previous reports,[6–10] that is, the oxygen deficiency results in the increase of ρ_0 and the left shift of T_C, from over 300 down to 195 K. This can be attributed to the decrease of carrier density caused by oxygen vacancies. However, as P_O approaching to 0.10 mbar ($P_O=0.11$, 0.10, 0.09, and 0.08 mbar), the sample transport behaviors deviate

[a]Electronic mail:scip8005@nus.edu.sg

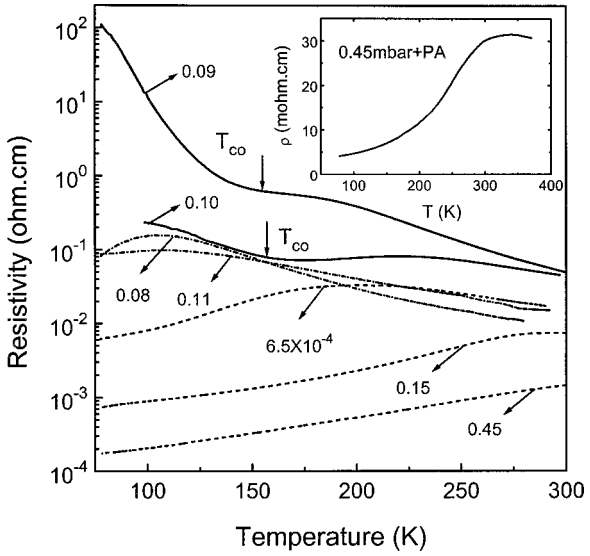

FIG. 1. Zero-field ρ_0-T curves of samples deposited at different P_O. The CO-transition temperature T_{CO} was indicated by arrows.

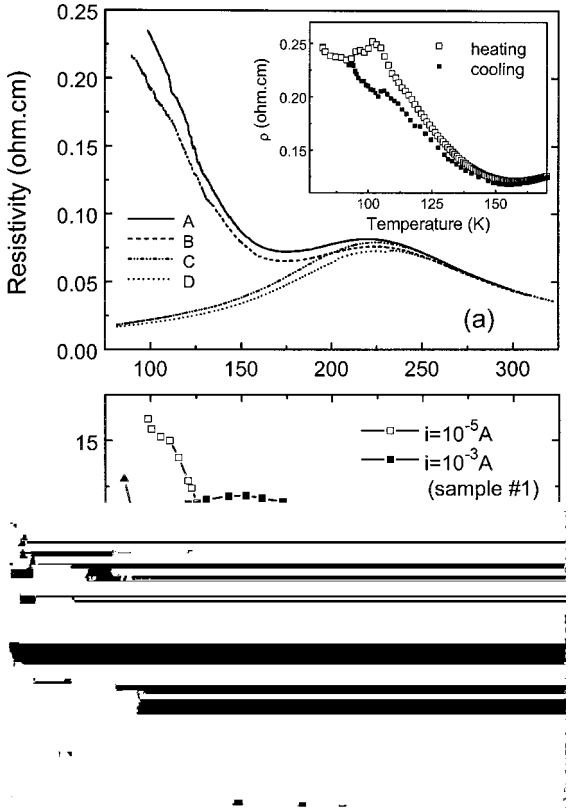

FIG. 2. (a) ρ-T curves of sample No.1 in zero field and 0.4 T for different I. (A: $\mu_0 H=0$ T, $I=10\,\mu$A; B: $\mu_0 H=0.4$ T, $I=10\,\mu$A; C: $\mu_0 H=0$ T, $I=1$ mA; D: $\mu_0 H=0.4$ T, $I=1$ mA.) Inset is the cooling and heating ρ_0-T curves measured using 10 μA in zero field. (b). The MR ratios of sample Nos. 1 and 2 measured in 0.4 T.

from the rule described earlier, suggesting the involvement of a new mechanism at this ambient. Especially for samples deposited at $P_O=0.10$ mbar (sample No. 1) and $P_O=0.09$ mbar (sample No. 2), there is a metal to insulator (M–I) transition at a temperature lower than T_C, accompanied by a dramatically resistivity growth. At $T=77$ K, resistivity of sample No. 2 is about five orders of magnitude higher than that of the sample deposited at $P_O=6.5\times10^{-4}$ mbar. This is a typical signature of a CO transition. In this letter we would like to attribute the CO transition recorded here to the lattice distortion or the W narrowness caused by oxygen deficiency.

Besides the M–I transition or the rapid resistivity growth, as observed, additional evidences of the CO transition may be found in either the thermal hysteresis measurement, referring to the first-order nature of the CO transition, or the ordering melting observation by applying external magnetic field, electric field or even x-ray radiation.[3,11–13] In Fig. 2(a) we show the transport behaviors of sample No. 1 at zero field and 0.4 T, respectively, as the current (I) flowing through the sample takes two different values. At $I=10\,\mu$A, the sample finds the insulator–metal transition temperature T_C at 220 K, which is attributed to the double exchange mechanism, and subsequently M–I transition temperature (T_{CO}) at 170 K, which we would like to attribute to CO transition in the present letter. As the current increase to 1 mA, the DE transition temperature T_C remains unchanged whereas the CO transition is, however, suppressed, leaving the metallic behavior down to 77 K. Due to the fact that the measurement current flowing through is proportional to the electric field applied to the sample, the absent of the high-resistivity state at low T as the current is increased can be considered as collapse of the CO state in a higher electric field. Additional heating and cooling experiments are performed and the thermal hysteresis observed is shown as the inset in Fig. 2(a). The heating ρ_0-T curve first retraces the cooling ρ_0-T curve, but soon jumps to a value higher than the corresponded cooling one, then follows a higher ρ_0 path. The two curves merge at a temperature near T_{CO}.

The MR ratio [defined as $(\rho(0)-\rho(0.4T))/\rho(0)$] derived from Fig. 2(a), for two different values of measurement current, is plotted in Fig. 2(b). At $I=10\,\mu$A, the MR-T curve is similar in shape with the related ρ_0-T curve, with a broad peak at the vicinity of T_C and a dramatic increase as $T<T_{CO}$. The MR value is as high as 15% at 90 K. The MR-T peak can be explained as a result of the right shift of T_C in a magnetic field. The extraordinary large MR value at low temperatures can be understood either as a result of left shift T_{CO} or simply as a result of partial melting of the CO state in a magnetic field. In contrast, the MR-T curve measured at $I=1$ mA has only one peak located near T_C. The low temperature MR value at this current is higher than expected for a normal DE metallic state. This suggests that the CO configuration may not be completely suppressed at the present electric field and can be further melted by a magnetic field.

The temperature dependent MR ratio for sample No. 2 is also given in the bottom panel of Fig. 2 where the measurement current is 0.1 μA. Similar to that of sample No. 1, the MR-T curve of sample No. 2 shows a broad peak around T_C and a rapid growth at low temperatures, indicating the partial melting of CO state at the presence of a magnetic field. However, the MR value at 77 K is about 12%, lower than that of sample No. 1. Correspondingly, no electric field effect on the CO transition is observed in sample No. 2. As I increases from 1 μA to 0.1 mA, the ρ-T curve remains unchanged. Therefore, the sample No. 2 is believed to be in a ''deeper'' CO state than sample No. 1, thus much harder to be melted by external magnetic or electric fields.

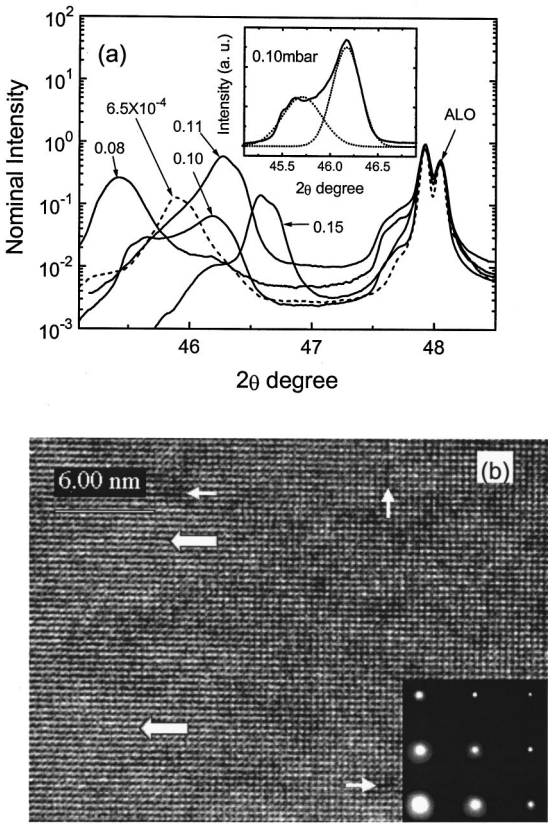

FIG. 3. (a) (002) reflections for films deposited at different P_O. Inset is the splitted (002) peak of the 0.10 mbar sample. (b) The planar section high-resolution lattice image for film deposited at $P_O = 6.5\times10^{-4}$ mbar. Defects are indicated by white arrows.

In addition, the microstructure of our films was examined using fine XRD and high-resolution transmission electron microscopy at room temperature. Figure 3(a) shows the local XRD pattern of the pseudocubic (002) reflection for films deposited at different P_O, as normalized by the respective ALO (002) reflections. The samples prepared at lower P_O have their (002) reflections at lower angles, corresponding to longer *c* axis. As the film deposited at 0.15 mbar has its *c* axis constant of 3.896 Å, that of the 0.08 mbar film is 3.990 Å. Therefore the *c*-axis extension of films deposited at reduced P_O is observed, which provides an indirect evidence of the correspondence between reduced P_O and oxygen deficiency in our films. One may note that the (002) peak of the film deposited at further reduced P_O (6.5×10^{-4} mbar) reverses the trend and goes back to a higher angle. A higher angle here is corresponding to a shorter *c*-axis, or a partially relieved lattice distortion. Rocking curve of the (002) reflection of the film shows full width at half maximum of 0.95°, much wider than that of the films deposited at higher P_O, which are among 0.5°–0.7°. This suggests that defects in the film deposited at $P_O = 6.5\times10^{-4}$ mbar is more serious. Instead of result in lattice distortion, the strain caused by the oxygen vacancies in this sample may be relieved by the formation of crystal defects.

This argument is further confirmed by the planar section high-resolution lattice image shown in the bottom panel of Fig. 3, where the incident electron beam is along the ⟨001⟩ of the pseudocubic lattice. Inset is the selected area electron diffraction. Point defects are observed, as indicated by the narrow arrows. A ''macroscopic'' crystal bending, as indicated by the thick arrows, can be attributed to a stacking fault. Therefore, the strain of the film is released in the form of crystal defects, such as dislocations and stacking faults, the Mn–O–Mn bond angle can keep a larger value, and so does the bandwidth *W*, thus the CO transition does not appear in the seriously oxygen deficient thin films.

Furthermore, the inset in Fig. 3(a) indicates that the (002) peak of the 0.10 mbar sample, where the CO state appears, is splitted. The curve can be fitted using two peaks, which correspond to the out-of-plane parameters of 3.967 and 3.929 Å, respectively, suggesting the existence of two phases. The phase separation revealed here might have some relationship with the CO transition, since the CO transition often accompanies a lattice parameter change.

The variation of magnetization with decreasing *T* in a field of 0.5 T, and the magnetization hysteresis loops at three different temperatures of sample No. 2 are also recorded (not shown here). Ferromagnetic (FM) behavior is observed over a wide temperature range from room temperature to 77 K (much lower than T_{CO}). The experiment data can be well understood by the coexistence of the FM state and the CO state in sample No. 2, since the existence of the CO state has already been verified by transport measurements earlier. In fact, direct evidence of the coexistence of the FM state and CO state have been demonstrated in $La_{5/8-y}Pr_yCa_{3/8}MnO_3$ system recently.[14] Other groups also argued coexistence that occurs as the short ranged CO-state matrix in the long ranged FM metallic network.[13,15] Future experiments such as temperature dependent XRD will be helpful to further clarify this issue.

J.M.L. acknowledges the partial supporty of NSFC, and the LSSMS of Nanjing University.

[1] H. Kawano, R. Kajimoto, H. Yoshizawa, Y. Tomioka, H. Kuwahara, and Y. Tokura, Phys. Rev. Lett. **78**, 4253 (1997).
[2] H. Kuwahara and Y. Tokura, *Colossal Magnetoresistance, Charge Ordering and Related Properties of Manganese Oxides* (World Scientific, Singapore, 1998), p. 217; S.-W. Cheong and C. H. Chen, *Charge Ordering and Related Properties of Manganese Oxides* (World Scientific, Singapore, 1998), p. 241.
[3] A. Arulraj, P. N. Santhosh, R. Srinivasa Gopalan, A. Guha, A. K. Raychaudhuri, N. Kumar, and C. N. R. Rao, J. Phys.: Condens. Matter **10**, 8497 (1998).
[4] Y. Tomioka, H. Kuwahara, A. Asamitsu, and M. Kasai, Appl. Phys. Lett. **70**, 3609 (1997).
[5] H. Y. Hwang, S.-W. Cheong, P. G. Radaelli, M. Marezio, and B. Batlogg, Phys. Rev. Lett. **75**, 914 (1995).
[6] K. M. Satyalakshmi, S. S. Manoharan, M. S. Hegde, V. Prasad, and S. V. Subramanyam, J. Appl. Phys. **78**, 6861 (1995).
[7] W. Zhang, W. Boyd, M. Elliot, and W. Herrenden-Harkerand, Appl. Phys. Lett. **69**, 3929 (1996).
[8] J.-M. Liu and C. K. Ong, Appl. Phys. Lett. **73**, 1047 (1998).
[9] R. Mahendiran, S. K. Tiwary, A. K. Raychaudhuri, and T. V. Ramakrishnan, Phys. Rev. B **53**, 3348 (1996).
[10] J.-M. Liu and C. K. Ong, J. Appl. Phys. **84**, 5560 (1998).
[11] V. Kiryukhin, Y. J. Wang, F. C. Chou, M. A. Kastner, and R. J. Birgeneau, Phys. Rev. B **59**, R6581 (1998).
[12] A. Asamitsu, Y. Tomioka, H. Kuwahara, and Y. Tokura, Nature (London) **388**, 50 (1997).
[13] V. Ponnambalam, S. Parashar, A. R. Raju, and C. N. R. Rao, Appl. Phys. Lett. **74**, 206 (1998).
[14] M. Uehara, S. Mori, C. H. Chen, and S. W. Cheong, Nature (London) **399**, 560 (1999).
[15] Y. Moritomo, A. Machida, S. Mori, N. Yamamoto, and A. Nakamura, Phys. Rev. B **60**, 9220 (1999).